Turbulence, Heat and Mass Transfer 7

LES/CMC of blow-off in a liquid fueled swirl burner

A. Tyliszczak[1] and E. Mastorakos[2]

[1]*Faculty of Mechanical Engineering and Computer Sci., Czestochowa University of Tech., Al. Armii Krajowej 21, 42-200 Czestochowa, Poland, atyl@imc.pcz.czest.pl*

[2]*Department of Engineering, Cambridge University, Cambridge CB2 1PZ, United Kingdom, em257@eng.cam.ac.uk*

Abstract — Large Eddy Simulations of two-phase combustion with the Conditional Moment Closure sub-grid model have been performed for flow conditions corresponding to stable and blow-off regimes in a swirl heptane spray burner. In the case of stable flame (i.e. low velocity), the predicted location and shape of the flame agree well with high-speed camera images from an experiment. Using model constants previously calibrated against pilot jet flame with localised extinction, we obtain that at the experimentally determined blow-off velocity, the predicted flame also blows-off, demonstrating that the LES/CMC can capture global extinction of a realistic flame.

1. Introduction

The extinction (or blow-off) process is a strongly unsteady phenomenon and therefore its experimental and numerical prediction is a very challenging task. It requires application of sophisticated experimental equipment or advanced combustion models accounting for the multiple interactions that occur between the liquid spray and the turbulent flow field. Experimental and numerical studies of strong unsteadiness in two-phase combustion mainly have focused so far on spark ignition phenomena. The ignition of an n-heptane spray in a bluff-body configuration was examined experimentally [1] and then it was simulated numerically using Large Eddy Simulations (LES) combined with Conditional Moment Closure (CMC) combustion model. The ignition together with the flame propagation in industrial combustion chamber was studied in [2] applying LES-Eulerian PDF approach.

Recently, an experimental analysis of combined ignition and blow-off processes of the n-heptane spray flame in a bluff-body swirl burner was done in [3] and the corresponding LES-CMC of ignition was performed in [4]. The present work extends this study and it focuses on the extinction phenomena using LES and CMC. In case of gaseous flows it was shown in [5, 6, 7] that LES-CMC is able to capture correctly the auto-ignition, local extinctions and re-ignition phenomena. The present paper aims to see if we can get localised extinction also for spray recirculating flames and also if we can correctly predict the global blow-off conditions.

2. Model formulation and numerical method

2.1. CMC for liquid fuels

The CMC equations for sprays can be obtained by conditional filtering of the transport equations or by applying jont PDF approach of Klimenko [8, 9]. In the limit of a dilute spray both derivations result in the identical equations given as [8]:

$$\frac{\partial Q_\alpha}{\partial t} + \widetilde{u_j|\eta}\frac{\partial Q_\alpha}{\partial x_j} = e_\alpha + \widetilde{N|\eta}\frac{\partial^2 Q_\alpha}{\partial \eta^2} + \widetilde{\dot{\omega}|\eta} + \delta_{\alpha,f}\widetilde{\Pi|\eta} - \left(Q_\alpha + (1-\eta)\frac{\partial Q_\alpha}{\partial \eta}\right)\widetilde{\Pi|\eta} \qquad (1)$$

where the operator $\widetilde{(\cdot|\eta)} = \widetilde{(\cdot|\xi=\eta)}$ stands for the density-weighted LES filtering conditioned on the mixture fraction ξ, see [10, 11]. The symbol $Q_\alpha = \widetilde{Y_\alpha|\eta}$ corresponds to the conditionally

filtered mass fraction of species α, and $\widetilde{u_j|\eta}$, $\widetilde{N|\eta}$, $\widetilde{\dot{\omega}|\eta}$ and $\widetilde{\Pi|\eta}$ are the conditionally filtered velocity, scalar dissipation rate, reaction rate and the mass evaporation rate. The Kronecker delta, $\delta_{\alpha,f}$ is equal to one for a fuel and zero otherwise. The equation for the conditionally filtered enthalpy, $Q_h = \widetilde{h|\eta}$, takes the form:

$$\frac{\partial Q_h}{\partial t} + \widetilde{u_j|\eta}\frac{\partial Q_h}{\partial x_j} = e_h + \widetilde{N|\eta}\frac{\partial^2 Q_h}{\partial \eta^2} + \widetilde{\Pi_h|\eta} - \left(Q_h + (1-\eta)\frac{\partial Q_h}{\partial \eta}\right)\widetilde{\Pi|\eta} \tag{2}$$

where the radiation and pressure work terms have been neglected. The terms e_α and e_h in Eq. (1) and Eq. (2) represent contributions from the subgrid scales and account for the conditional transport in the physical space and also in the mixture fraction space due to presence of evaporation source terms. The conditionally filtered terms, $\widetilde{\Pi|\eta}$ in Eq. (1) and $\widetilde{\Pi_h|\eta}$ in Eq. (2), are responsible for the mass and heat exchange between gas and liquid. The are related to their unconditional counterparts defined as: $\widetilde{\Pi} = \frac{1}{V}\sum_{i=1}^{N_d} dm_i/dt$, $\widetilde{\Pi}_h = \frac{1}{V}\sum_{i=1}^{N_d} \frac{d(m_i C p_L \theta_i)}{dt}$ where V is the volume of the computational cell, N_d is the number of liquid droplets in that cell, the symbols m_i and θ_i are the mass and temperature of i-th droplet, and Cp_L is the heat capacity of the fuel.

The terms e_α, e_h, $\widetilde{\dot{\omega}|\eta}$, $\widetilde{u_j|\eta}$, $\widetilde{N|\eta}$ as well as the source terms $\widetilde{\Pi_h|\eta}$ and $\widetilde{\Pi|\eta}$ are unclosed and require modelling. In the presence of spray the terms e_α and e_h are defined as:

$$e_\alpha = -\frac{1}{\overline{\rho}\,\widetilde{\mathcal{P}}(\eta)}\frac{\partial}{\partial x_j}\left[\overline{\rho}\widetilde{\mathcal{P}}(\eta)\,\widetilde{u_j'' Y_\alpha''|\eta}\right] - \frac{1}{\overline{\rho}\,\widetilde{\mathcal{P}}(\eta)}\frac{\partial}{\partial \eta}\left[\overline{\rho}\widetilde{(1-\eta)}\mathcal{P}(\eta)\,\widetilde{Y''\Pi''|\eta}\right] \tag{3}$$

$$e_h = -\frac{1}{\overline{\rho}\,\widetilde{\mathcal{P}}(\eta)}\frac{\partial}{\partial x_j}\left[\overline{\rho}\widetilde{\mathcal{P}}(\eta)\,\widetilde{u_j'' h''|\eta}\right] - \frac{1}{\overline{\rho}\,\widetilde{\mathcal{P}}(\eta)}\frac{\partial}{\partial \eta}\left[\overline{\rho}\widetilde{(1-\eta)}\mathcal{P}(\eta)\,\widetilde{h''\Pi''|\eta}\right] \tag{4}$$

The conditional joint fluctuations of evaporation rate with species and enthalpy fluctuations are assumed to be negligible, and hence the second term on the right hand side of Eqs.(3) and (4) is neglected. With the assumption of equal diffusivity for all reactive scalars, the joint conditional fluctuations of velocity and species are modelled with a gradient model [10], i.e. $\widetilde{u_j'' Y_\alpha''|\eta} = -D_t\frac{\partial Q_\alpha}{\partial x_i}$ and analogous expression for the joint conditional enthalpy-velocity fluctuations. The turbulent diffusivity is computed as $D_t = \nu_t/Sc_t$ where ν_t is the turbulent subgrid viscosity and the turbulent Schmidt number equals $Sc_t = 0.4$. The chemical reaction rate is modelled by first order closure [9]: $\widetilde{\dot{\omega}|\eta} = \dot{\omega}_\alpha\,(Q_1, Q_2, ..., Q_n, Q_h)$, where n is the number of reacting scalars. The conditional velocity may be modelled by a linear model [9] or by explicit conditional filering [10] or assumed constant [11]. There is no evident advantage of any approach, therefore we assumed the conditional velocity uniform in η-space and equal to the local filtered velocity, i.e. $\widetilde{u_j|\eta} = \widetilde{u}_j$, similarly as in [11].

Modelling of $\widetilde{\Pi|\eta}$ for two-phase flows was proposed in [12] in the context of RANS approach and it was further extended to LES for modelling of spark ignition of liquid fuel [4]. The model for $\widetilde{\Pi|\eta}$ was defined as:

$$\widetilde{\Pi|\eta} = \widetilde{\Pi}\,\delta(\eta - \bar{\xi}_s)/\mathcal{P}(\bar{\xi}_s) \tag{5}$$

where ξ_s is the value of the fuel mass fraction at saturation (evaluated at the droplet temperature) and $\mathcal{P}$ is the filtered density function of the mixture fraction. Modeling of $\widetilde{\Pi_h|\eta}$ is based on the formula analogous to Eq. (5) but with $\widetilde{\Pi} \to \widetilde{\Pi}_h$.

The conditional scalar dissipation $\widetilde{N|\eta}$ is given as:

$$\widetilde{N|\eta} = C_N \frac{1}{2} \frac{\nu_t}{\Delta^2} \widetilde{\xi''^2} \tag{6}$$

where the model for the mixture fraction variance is formulated as [4]:

$$\bar{\rho}\widetilde{\xi''^2} = \left(C_V \bar{\rho} \Delta^2 \frac{\partial \widetilde{\xi}}{\partial x_j} \frac{\partial \widetilde{\xi}}{\partial x_j} + \frac{\Delta^2}{\nu_t} \widetilde{\xi'' \Pi''} \right) \quad , \quad \widetilde{\xi'' \Pi''} = \widetilde{\xi \, \Pi} - \widetilde{\xi} \, \widetilde{\Pi} = \bar{\xi}_s \widetilde{\Pi} - \widetilde{\xi} \widetilde{\Pi} \tag{7}$$

where $\widetilde{\xi}$ is the filtered mixture fraction. The constant C_V in Eq. (7) is equal to 0.1 as suggested in [13] for gaseous flows. More questionable is the value of the constant C_N in Eq. (6) as there are not clear advises what it should be, it turns out that depending on the flow problem it varies considerably. For instance, in the LES-CMC simulations of hydrogen autoignition [14, 7] or methane bluff body stabilized flame [15] C_N was assumed of the order of $\mathcal{O}(1)$ whereas in prediction of the local extinction [6] they assumed $C_N = 42$ as the result of calibration for Sandia flame D. In the present paper it is demonstrated that C_N may have a crucial influence on the flow field behavior.

2.2. LES solver and solution strategy

The CMC model was implemented in a 2nd order finite-volume code PRECISE [16] (unstructured version) with an implicit 2nd order integration method in time. The simulations were performed with the Smagorinski subgrid model. The liquid phase was tracked using a Lagrangian formulation where the fuel droplets are presumed to act as point sources of mass and momentum that modify the vapour fuel distribution, depending on the gas velocity, temperature, pressure and the vapour mass fraction [17, 18, 19].

The CMC model is very expensive computationally and therefore a typical approach bases on application of two separate meshes, i.e. one for the flow field and the second (coarse) for the CMC equations, see [11] for details of implementation issues of the CMC model. In the simulations performed in this work, the CFD and CMC meshes consisted of 3×10^6 and 54000 cells respectively. The CMC equations were solved applying the operator splitting approach where the transport in physical space, transport in mixture fraction space and chemistry terms are solved separately thus reducing the number of equations solved simultaneously. The second order terms in physical and mixture fraction spaces were discretized with 2nd order central difference method. The TVD scheme with van Leer limiters [20] was applied for the convective terms in physical space. The numerical time step was assumed constant and equal to $\Delta t = 5.0 \times 10^{-6}$ s, which on the CFD mesh resulted in CFL number oscillating around 0.2. The same time step was used for droplets tracking and for the CMC model. The CMC mesh is coarser than CFD one and this yields even smaller CFL number on the CMC mesh. Therefore, the CMC equations in physical space were integrated in time applying a first order explicit Euler method. However, expecting high velocity fluctuations during possible local extinctions or blow-off, the explicit integration procedure was supplemented with an automatic time step reduction algorithm. The numerical mesh in mixture fraction space consisted of 51 nodes stretched in the vicinity of the stoichiometric mixture fraction, which is equal to 0.06. In mixture fraction space the time integration was fully implicit. The 2nd order discretization applied for the difusive terms resulted in the tri-diagonal system that was solved with the TDMA algorithm.

The last step of the splitting procedure was the solution of the CMC equations with the chemical terms, and at this stage a VODPK [21] solver (designed for the stiff systems) was

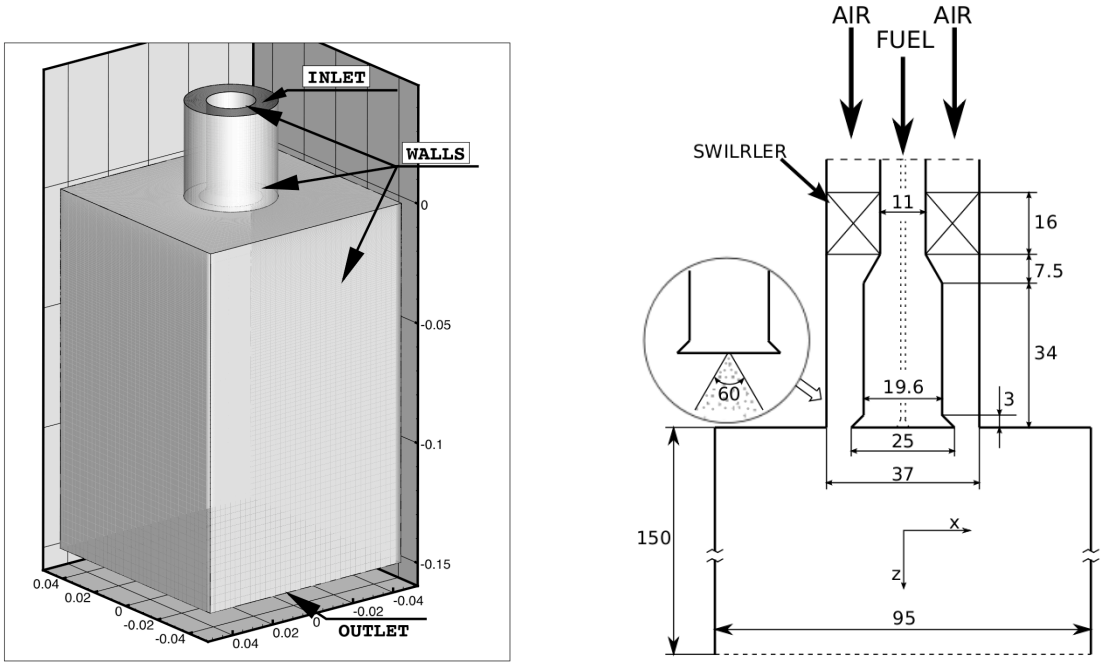

Figure 1: The computational domain with the boundary conditions (left figure) and sketch showing detailed dimensions of the bluff-body and combustion chamber [3].

applied. The chemical reaction was modelled by a modified one-step chemistry for heptane, following the method proposed [22] which is based on a tuning of the heat release rate as a function of the local equivalence ratio to give approximately the correct flame speed and temperature across the whole flammable range.

3. Results and discussion

The computational domain is shown in Fig. 1. It consisted of a circular duct of inner diameter $D = 37$ mm fitted with a conical bluff body of diameter $D_b = 25$ mm. A 60° swirler was located 40 mm upstream of the bluff body. A hollow-cone atomiser was placed inside the bluff body and the liquid fuel (heptane) was injected through a slot of 0.15 mm diameter. In the simulations the injections was modelled by 64 discrete injection points uniformly distributed along the circle with 0.15 mm diameter. Analysed cases included stable combustion regimes (in the following denoted as SWH1) with air bulk velocity $U_b = 14.3$m/s, and blow-off conditions (denoted as SWH3) with $U_b = 18.5$m/s that corresponded to the experimental blow-off point [3].

3.1. LES verification for cold flow

Prior to the analysis of the flame behaviour in the blow-off regimes, the accuracy of the LES code, the boundary conditions and the mesh density were verified for the cold flow conditions (no flame, no spray) for which detailed measurements of the velocity exist [23]. The profiles of mean axial and tangential velocity components are shown in Fig. 2 - 3 for the SWH1 and SWH3 conditions, and RMS of axial and tangential components in Fig. 4 for the SWH1 conditions. The negative values of the axial velocity in the center of the domain correspond to the recirculation zone where the flow direction is oriented towards the bluff-body. The recirculation zone extends downstream and almost reaches the end of the domain. The profiles of the mean velocity presented in Fig. 2 - 3 are in very good agreement with the experimental data both

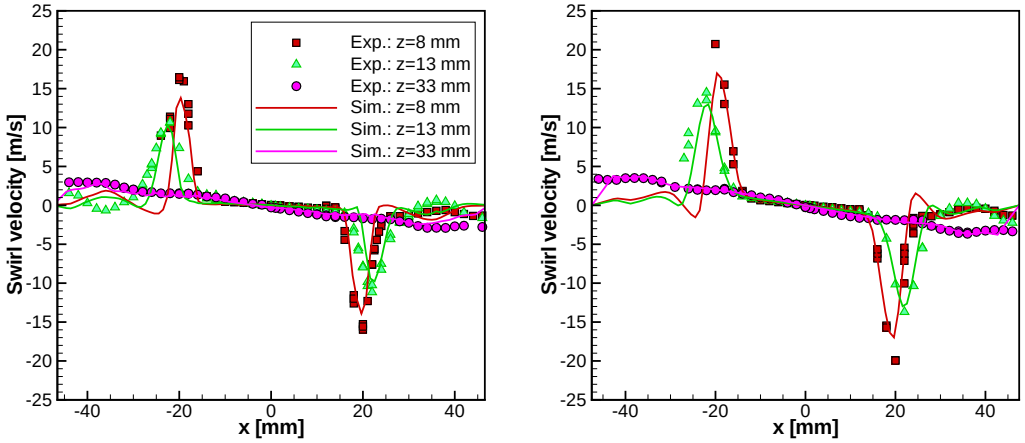

(a) SWH1 (b) SWH3

Figure 2: Radial profiles of the mean **tangential** velocity for SWH1 and SWH3 conditions at different stations at the indicated distance from the bluff-body. The symbols refer to the experimental data [3].

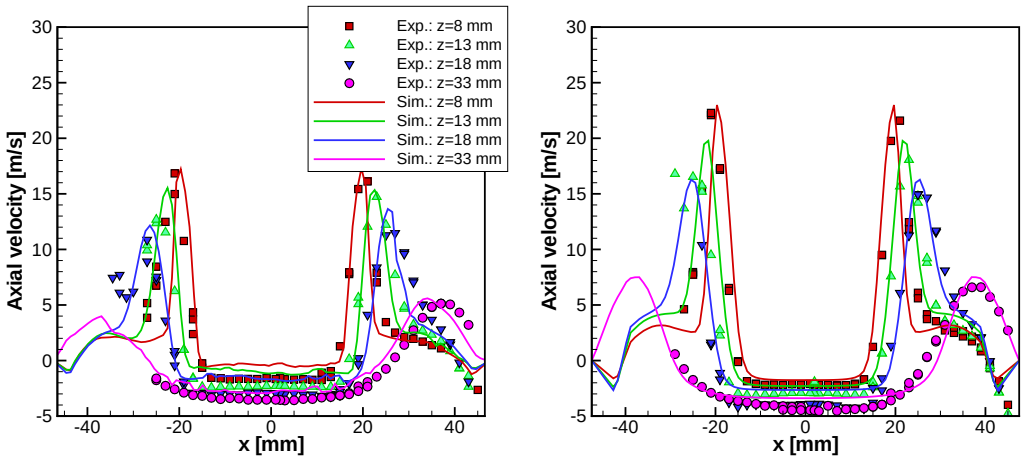

(a) SWH1 (b) SWH3

Figure 3: Radial profiles of the mean **axial** velocity.

close to the bluff body at a distance $z = 8\,\text{mm}$ as well as further downstream at $z = 33\,\text{mm}$. The RMS values are slightly underpredicted, particularly in the center of the domain. However, the trend is well captured, and hence, one may conclude that the aerodynamics in the burner are captured well, although it was assessed for the cold flow conditions only.

3.2. Blow-off regimes

Modelling of the blow-off regimes started from the cold flow conditions SWH1, then the liquid fuel was injected and after a while the spray spread in the whole domain. The combustion was initiated by a numerical spark modelled by prescribing a "burning flamelet solution" in $3 \times 3 \times 3$ CMC cells from which the flame developed in the chamber. Figure 5 shows the heat release value $(60\text{MJ/m}^3\text{s})$ in selected time instants $(\Delta T = 0.005\text{s})$ during the flame propagation. Finally, the flame stabilizes in about 20ms and remains attached to the bluff-body.

In the next step the velocity of the inlet air was smoothly increased up to $U_b = 18.5\text{m/s}$ that

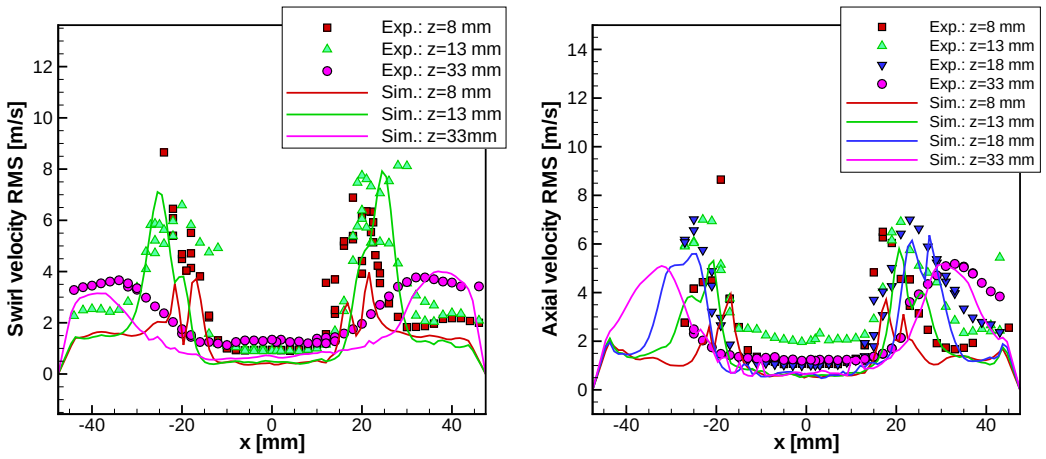

(a) RMS of **tangential** velocity (b) RMS of **axial** velocity

Figure 4: Radial profiles of the RMS of **tangential** and **axial** velocity for SWH1 conditions.

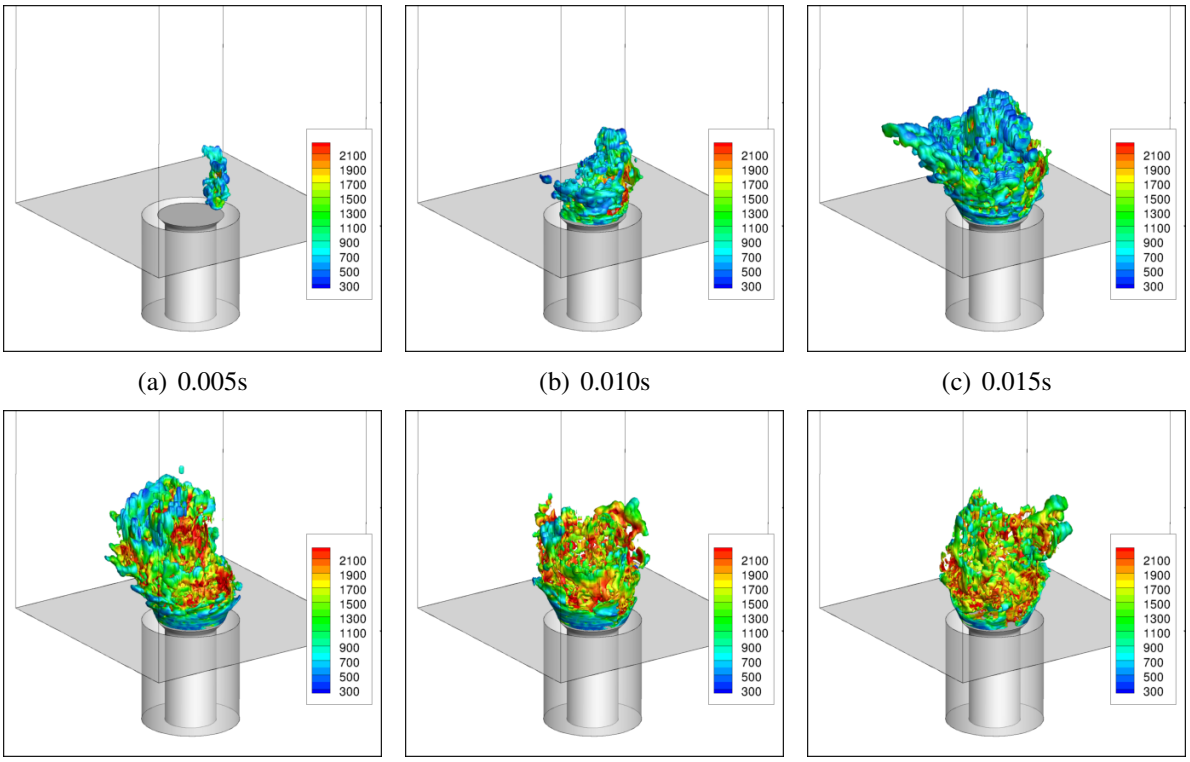

(a) 0.005s (b) 0.010s (c) 0.015s

(d) 0.020s (e) 0.025s (f) 0.030s

Figure 5: Isosurface of the heat release $(60\mathrm{MJ/m^3s})$ at selected time instants after the ignition. Colors correspond to the temperature.

corresponded to the experimental blow-off regimes. The change of the boundary conditions was done in a short time, i.e. 0.005ms, but it does not imply that the entire flow field "felt" this modification immediately. From the calculations performed for the cold flow conditions we estimated that in the vicinity of the bluff-body ($1D_B - 2D_B$) the flow field fully adapts to the new boundary conditions after 0.035s approximately. Assuming that in the presence of the flame the flow behaves similarly, the computations had to last for that period of time and only then one could expect occurrence of the local extinctions or blow-off.

During the ignition and the transient phases the computations were performed with the constant $C_N = 2$ in Eq. (6). Sample results showing the predicted temperature contours and data form OH-PLIF measurements overlapped with Mie-scattering (white lines) data are shown in Fig. 6. The white isolines in the computational results (figure on the left hand side in Fig. 6) represent the contours of the liquid volume concentration which indicates the location of the droplets. Numerical results show that the inertia of the droplets is very high and their spreading rate is very small. This causes that the droplets follow trajectories along the injection angle for a long distance. Although a very similar behaviour is seen in the experimental data, the computational results seem to be more narrow. This may result from the fact that in the computations the droplets are injected without any randomness, neither in the location nor in the velocity. In the experiment the droplets are injected through the circular slot whereas in the computations from 64 uniformly distributed holes with deterministic velocity without fluctuations.

The letters A1, A2, B1, B2 denote locations of the nodes of the CMC mesh where the solution was analysed in mixture fraction space. Point A1 lies at the shear layer between the recirculation zone and the stream of inlet air. Point A2 lies in the stream of the droplets. Points B1 and B2 are located on the edge of the flame. Strong variations of the solution at B-points would indicate movement of the flame front. The results in points A1, A2, B1, B2 are presented in Fig. 7 showing time variations of the conditional temperature and conditional scalar dissipation rate (SDR) at the stoichiometric mixture fraction 0.06. Except for point A2 the conditional temperature changes very little, the SDR is very low and the temperature remains high. The solution in the point A2 show strong and lasting relatively long (appr.1ms) variations of both the SDR and temperature. This could be interpreted as a sign of the local extinction but even if this is the case the solution stabilizes and the flame remains stable for the rest of the simulation time. Figure 8 shows instantaneous isosurfaces of the stoichiometric mixture fraction colored by the temperature. The "holes" in these isosurfaces correspond to the temperature below 600K, for better visibility the holes were surrounded by the black line. Clearly there are very few places with the temperature falling below 600K, the flame is stable and certainly far from extinction.

Further analysis showed that the flame behaviour changes depending on the way of computing the SDR and a way of transferring its values from the CFD mesh to the CMC mesh. Various alternative tests included using the AMC model applied on the CFD mesh, the AMC model applied on the CMC mesh, and various possibilities of the volume averaging, see [11]. Here one should note that applying AMC model for SDR always leads to a bell-shape distribution scaled by some maximum value. Indeed, it turned that this maximum was the most influencing parameter.

Similar conclusions were formulated in [6] in the case of the LES-CMC simulations of methane diffusion flames. There, it was shown that the local extinctions are very sensitive to the scalar dissipation level - they managed to capture the extinctions by adjusting the model constant according to experimental data, i.e. setting $C_N = 42$ instead of generally assumed $C_N = 2$. Obviously, this increased the level of SDR significantly. In the present configuration the experimental data do not include measurements of the SDR. Therefore the next computa-

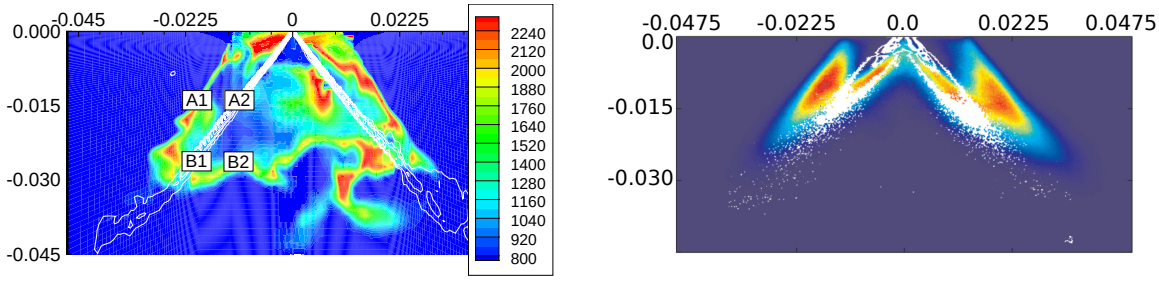

(a) computations (b) experiment

Figure 6: Left figure: contours of the temperature in the $(x - z)$ cross-section plane; white isolines in the left figure represent contours of the liquid volumetric concentration. Right figure (experimental data [24]): Mie scattering (white contours) and OH-PLIF (color map).

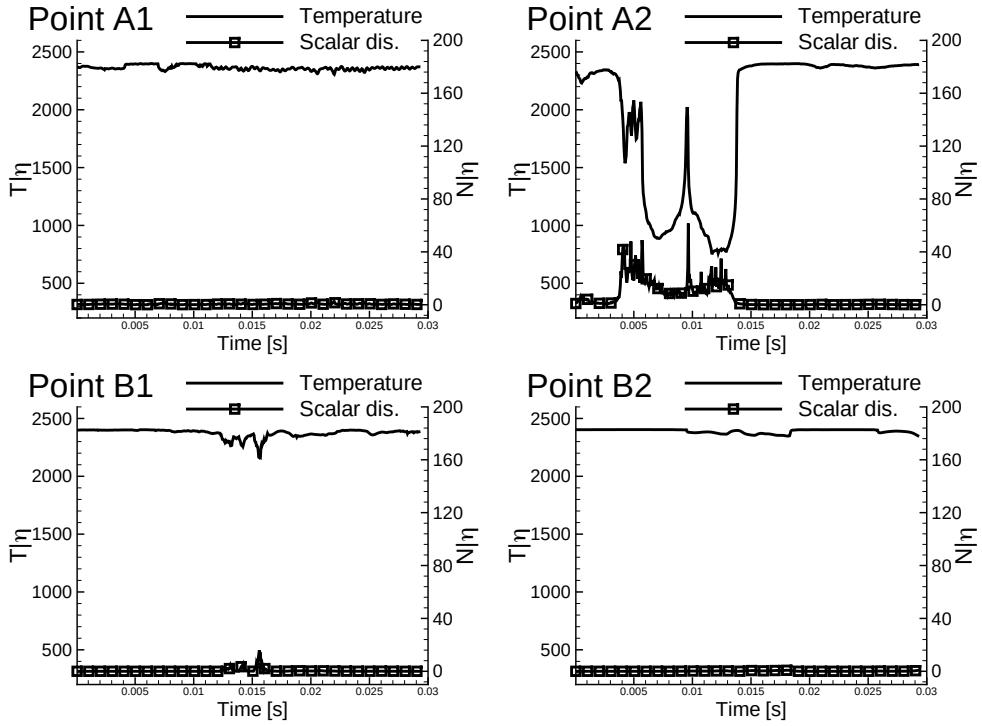

Figure 7: Time variations of the conditional temperature and scalar dissipation rate at the stoichiometric mixture fraction. Solution with $C_N = 2$ in Eq. (6).

tions were performed with $C_N = 42$, although the flow problem considered here and in [6] are drastically different. The initial solution for computations with $C_N = 42$ was the one obtained previously for $C_N = 2$ and stored at the time 0.014s (see Fig. 7 and Fig. 8). The constant C_N had to be increased progressively, i.e. a few hundreds of time steps had to be performed with $C_N = 20$, then with $C_N = 30$, and finally we could set $C_N = 42$. This procedure was necessary due to stability problem - the solver diverged when C_N risen to much in a single time step. The solutions shown in Fig. 9 present the conditional temperature and SDR in the same points as before. Except for the point B2 the effect of alteration of C_N is evident. The temperature and SDR substantially vary in time. One may notice that the inertia of the CMC solution is very low, i.e. a change of the SDR causes almost immediate change of the conditional temperature. This has direct consequences for the resolved temperature and also density which almost immediately influence on the flow field and the shape of the flame. Figure 10 shows the isosurfaces of the stoichiometric mixture fraction, where as before the holes represent the local excitations. Evidently the flame exhibits very unstable behavior and as the time progress the flame seems to vanish starting from the left side of the bluff-body. In the experimental work [25] where the blow-off regimes were analysed based on OH^* chemiluminescence, it was found that the blow-off event is a relatively slow process. Based on six blow-off events the average blow-off time was estimated as 12ms. In the present computations this period of time corresponds to the solutions presented in Fig. 10, more or less. Although the flame still exists it seems that it approaches the global extinction.

Finally we compare the magnitude of the terms of the CMC equation for heptane. Figure 11 shows profiles of the diffusion term ($\frac{\partial}{\partial x_i}(D_t \frac{\partial Q_\alpha}{\partial x_i})$), the convection term ($\widetilde{u_j|\eta} \frac{\partial Q_\alpha}{\partial x_j}$), the diffusion in mixture fraction space ($\widetilde{N|\eta} \frac{\partial^2 Q_h}{\partial \eta^2}$), and the conditional scalar dissipation rate. The various lines represent the solutions collected with the time distance $\Delta T = 5 \times 10^{-5}$ at the point A2. In this location the droplets evaporate extensively which causes strong spatial gradients. However, the diffusion term in mixture fraction is at least one order of magnitude bigger then the convection and diffusion terms in physical space. The magnitude of the diffusion term is directly related to the SDR, which is shown in Fig. 11d where the red profile denotes the extinction limit determined in the 0D-CMC calculations, i.e. without the transport in physical space. Generally the scalar dissipation is high but most of the time it is below the extinction value. This suggests that even if the term ($\widetilde{N|\eta} \frac{\partial^2 Q_h}{\partial \eta^2}$) contributes the most in the CMC equation it may be not sufficient to cause extinction. There must be a combined mechanism (physical space - mixture fraction space) which causes that the flame extinguishes in the large part of the computational domain.

4. Conclusions

The results obtained here show that LES-CMC approach offers a way to capture the localized extinction and probably the global blow-off phenomena in non-premixed two-phase systems. Using model constants previously calibrated against pilot jet flames with localised extinction, we obtain that the predicted flame approaches extinction at the experimentally determined blow-off velocity. The simulations indicate a very important role for the modelling of the scalar dissipation rate, which turned out to be a key parameter influencing the model predictions. Further developments and validation are certainly needed to achieve a greater accuracy.

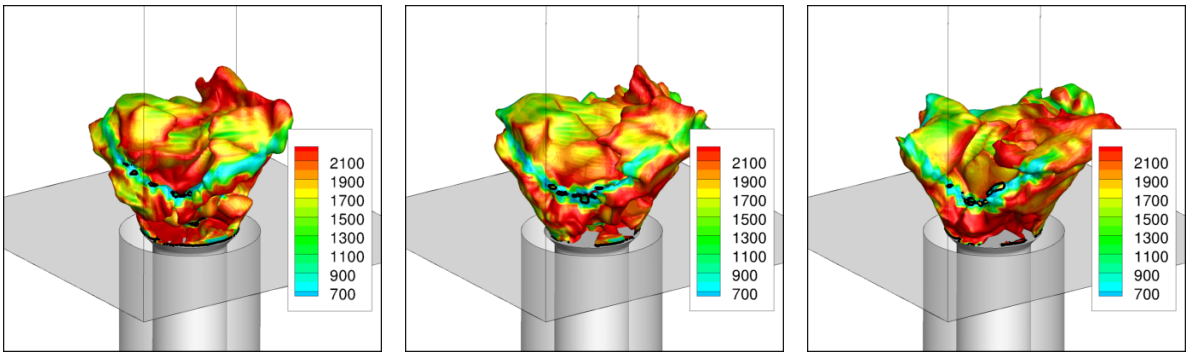

(a) Time: 0.0145s (b) Time: 0.0170s (c) Time: 0.0195s

Figure 8: Instantaneous isosurfaces of the stoichiometric mixture fraction with the model constant $C_N = 2$. Time instants are consistent with plots in Fig. 7. The colors denote the temperature.

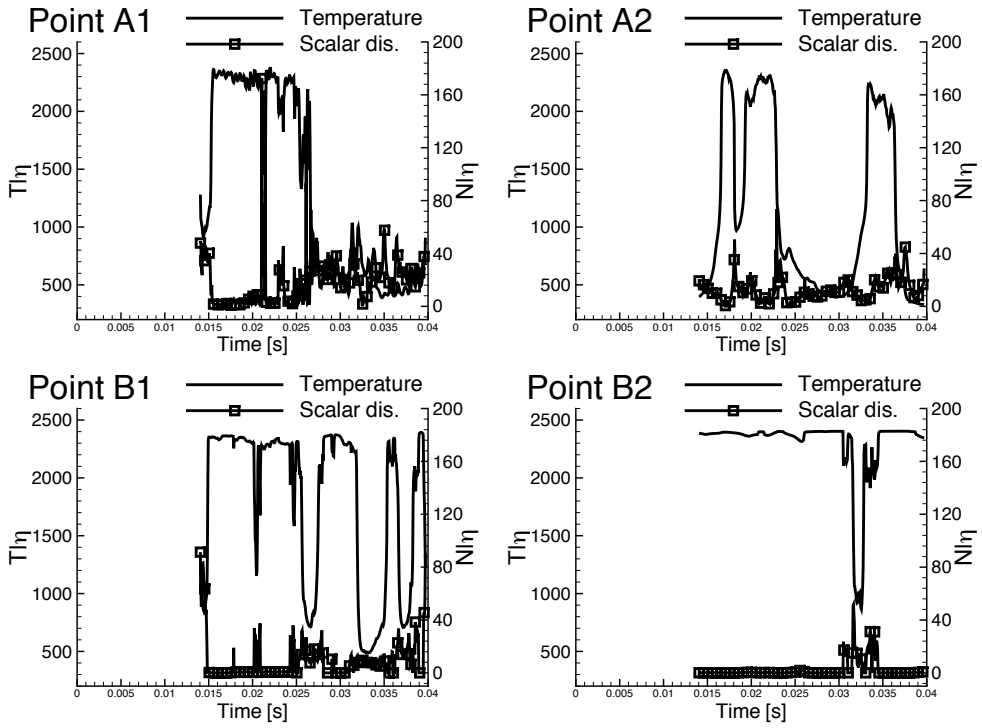

Figure 9: Time variations of the conditional temperature and scalar dissipation rate at the stoichiometric mixture fraction. Solution with $C_N = 42$ in Eq. (6).

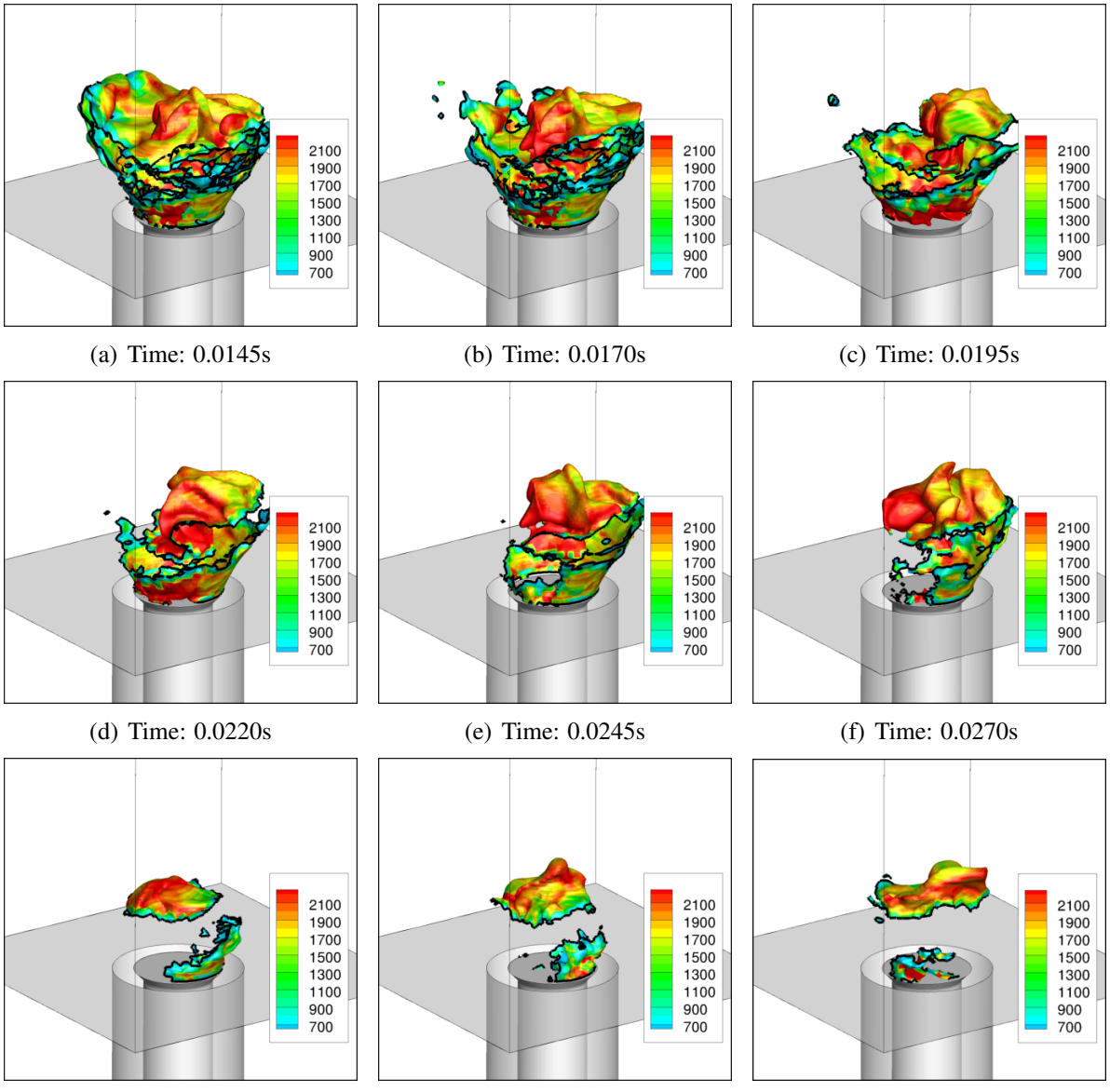

(a) Time: 0.0145s (b) Time: 0.0170s (c) Time: 0.0195s

(d) Time: 0.0220s (e) Time: 0.0245s (f) Time: 0.0270s

(g) Time: 0.0345s (h) Time: 0.0370s (i) Time: 0.0395s

Figure 10: Isosurface of the stoichiometric mixture fraction with the model constant $C_N = 42$.

Acknowledgements

This work has been funded by the European Commission (Project "MYPLANET"). The first author is grateful to Cyfronet Computer Center for access to PL-Grid infrastructure.

References

1. T. Marchione, S.F. Ahmed, E. Mastorakos. Ignition of turbulent swirling n-heptane spray flames using single and multiple sparks. *Combustion and Flame*, 156:166–180, 2009.
2. W. P. Jones, A. Tyliszczak. Large Eddy Simulation of spark ignition in a gas turbine combustor. *Flow, Turbulence and Combustion*, 85:711–734, 2010.
3. C. Letty, E. Mastorakos, A.R. Masri, M. Juddoo and W. O′Loughlin. Structure of igniting ethanol and n-heptane spray flames with and without swirl. *to app. in Exp. Therm. Fluid Sci.*
4. A. Tyliszczak, E. Mastorakos. LES/CMC predictions of spark ignition probability in a liquid fuelled swirl combustor. In *51st AIAA Aerospace Sciences Meeting*, submitted.
5. W. P. Jones, V. N. Prasad. Large Eddy Simulation of the Sandia Flame Series (D, E and F) using the Eulerian stochastic field method. *Combustion and Flame*, 157:1621–1636, 2010.
6. A. Garmory, E. Mastorakos. Capturing localised extinction in Sandia flame F with LES-CMC. *Proceedings of the Combustion Institute*, 33:1673–1680, 2011.
7. S. Navarro-Martinez, A. Kronenburg. Flame stabilization mechanism in lifted flames. *Flow, Turbulence and Combustion*, 87:377–406, 2011.
8. M. Mortensen, R.W. Bilger. Derivation of the conditional moment closure equations for spray combustion. *Combustion and Flame*, 156:62–72, 2009.
9. Y.A. Klimenko, R.W. Bilger. Conditional Moment Closure for turbulent combustion. *Prog. Energy Combust. Sci.*, 25:595–687, 1999.
10. S. Navarro-Martinez, A. Kronenburg, F. di Mare. Conditional moment closure for large eddy simulations. *Flow, Turbulence and Combustion*, 75:245–274, 2005.
11. A. Triantafyllidis, E. Mastorakos. Implementation issues of the Conditional Moment Closure in Large Eddy Simulations. *Flow, Turbulence and Combustion*, 84:481–512, 2009.
12. G. Borghesi, E. Mastorakos, C.B. Devaud, R.W. Bilger. Modeling evaporation effects in conditional moment closure for spray autoignition. *Combustion Theory and Modelling*, 15:725–752, 2011.
13. N. Branley and W. P. Jones. Large Eddy Simulation of a Turbulent Non-premixed Flame. *Combustion and Flame*, 127:1914–1934, 2001.
14. Stankovic I., Triantafyllidis A., Mastorakos E., Lacor C., Merci B. Simulation of hydrogen autoignition in a turbulent co-flow of heated air with LES and CMC approach. *Flow, Turbulence and Combustion*, 86:689–710, 2011.
15. A. Triantafyllidis, E. Mastorakos, R.L.G.M. Eggels. Large Eddy Simulations of forced ignition of a non-premixed bluff-body methane flame with Conditional Moment Closure. *Combustion and Fame*, 156:2328–2345, 2009.
16. S. James, J. Zhu, M.S. Anand. Large-Eddy Simulations as a Design Tool for Gas Turbine Combustion Systems. *AIAA Journal*, 44:674–686, 2006.
17. R. S. Miller, K. Harstad, J. Bellan. Evaluation of equilibrium and non-equilibrium evaporation models for many-droplet gas-liquid flow simulations. *International Journal of Multiphase Flow*, 24:1025–1055, 1998.
18. S. V. Apte, K. Mahesh, P. Moin. Large eddy simulations of evaporating spray in a coaxial combustor. *Proceedings of the Combustion Institute*, 32:2247–2256, 2009.
19. W. P. Jones, S. Lyra, A.J. Marquis. Large eddy simulation of evaporating kerosene and acetone sprays. *International Journal of Heat and Mass Transfer*, 53:2491–2505, 2010.
20. Hirsh Ch. *Numerical computation of internal and external flows*. JOHN WILEY & SONS, Chichester, 1990.
21. P.N. Brown, A.C. Hindmarsh. *Journal of Applied Math. Comp.*, 31:40–91, 1989.

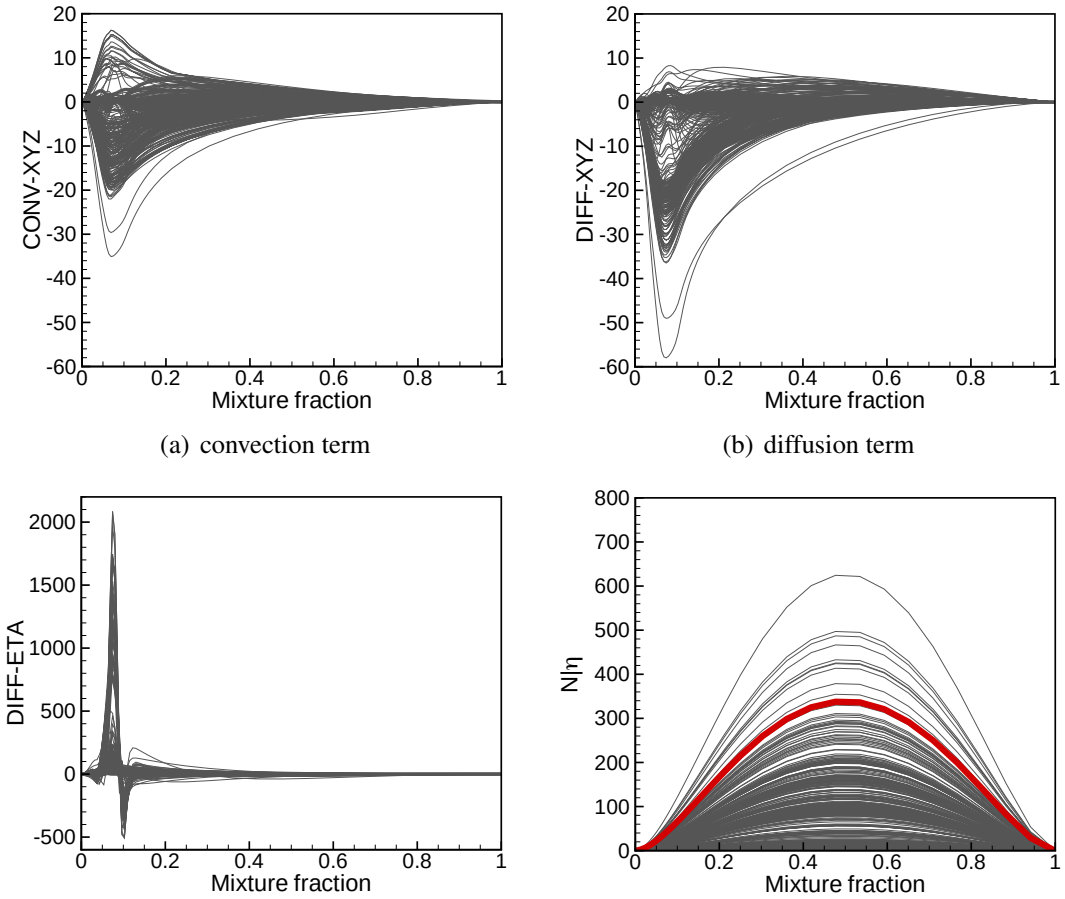

(a) convection term

(b) diffusion term

(c) diffusion in the mixture fraction space

(d) scalar dissipation rate

Figure 11: Terms of the CMC equation for heptane. Each line represents solution in a particular time instant with $\Delta T = 5 \times 10^{-5}$ s.

22. E. Fernández-Tarrazo, A.L. Sánchez , A. Liñán, F.A. Williams. A simple one-step chemistry model for partially premixed hydrocarbon combustion. *Combustion and Flame*, 147:32–38, 2006.
23. C. Letty, E. Mastorakos, M. Juddoo, W. O'Loughlin, A. R. Masri. Laser spark ignition and flame expansion in swirl burners fuelled with n-heptane sprays. In *Proceedings of th 23th ICDERS Conference*, 2011.
24. D.A. Cavaliere. private communication.
25. D.E. Cavaliere, J. Kariuki, E. Mastorakos. Blow-off behaviour of swirl-stabilized spray flames for different liquid fuels. In *51st AIAA Aerospace Sciences Meeting*, submitted.